Stratocumulus over SouthEast Pacific: Idealized 2D simulations with the Lagrangian Cloud Model

M. Andrejczuk, A. Gadian, A. Blyth

Corresponding Author:
M. Andrejczuk
M.Andrejczuk@leeds.ac.uk

School of Earth and Environment
University of Leeds
Leeds, LS2 9JT
January 12, 2012

Abstract

In this paper a LES model with Lagrangian representation of microphysics is used to simulate stratucumulus clouds in idealized 2D setup based on the VOCALS observations. The general features of the cloud simulated by the model, such as cloud water imixing ratio and cloud droplet number profile agree well with the observations. The model can capture observed relation between aerosol distribution and concentration measured below the cloud and cloud droplet number. Averaged over the whole cloud droplet spectrum from the numerical model and observed droplet spectrum are similar, with the observations showing a higher concentration of droplets bigger than 25 μm. Much bigger differences are present when comparing modelled and observed droplet spectrum on specific model level.

Despite the fact that microphysics is formulated in a Lagrangian framework the standard deviation of the cloud droplet distribution is larger than 1 μm. There is no significant narrowing of the cloud droplet distribution in the up-drafts, but the distribution in the up-drafts is narrower than in the down-drafts. Modelled and observed standard deviation profiles agree well with observations for moderate/high cloud droplet numbers, with much narrower than observed droplet spectrum for low idroplet number.

Model results show that a significant percentage of droplets containing aerosol bigger than 0.3 μm didn't reach activation radius, yet exceeding 1 μm, what is typically measured as a cloud droplets. Also, the relationship between aerosol sizes and cloud droplet sizes is complex; there is a broad range of possible cloud droplet sizes for a given aerosol size.

1. Introduction Microphysics parametrization is still an unresolved problem in numerical models. The large number of aerosol particles and cloud droplets in the atmosphere force the use of the simplified description of this process. The simplest approaches, single moment bulk models (Kessler, 1969), assume that the cloud is in equilibrium with the air. Water condenses/evaporates within one time-step and the final state is determined by the thermodynamic conditions. These type of models evolved to multi-moment models predicting not only the mass of the water, but also the number of droplets (Koenig and Murray 1976; Ferrier 1994; Meyers et al. 1997; Khairoutdinov and Kogan 2000; Seifert and Beheng 2001; Milbrandt and Yau 2005; Morrison et al. 2005). In the bulk approach, since the droplet spectrum is not predicted there is a problem with determining the amount of the water transported from the cloud by precipitation and how fast this transport proceeds. Although bulk models provide some useful information their applications, especially, when precipitation is present or information about spectrum is important is limited. Such models, however, are widely used due to their simplicity and fast execution.

Spectrum predicting models, bin models, replace the discrete description of individual cloud droplets with its continuous counterpart and are used in numerical models since 1970's. There are variety of such models (Leroy et al. 2009; Ackerman et al. 2004; Khain et al. 2004; Khairoutdinov and Kogan 1999) differing in the way droplet activation/deactivation is handled and how condensational growth and collision operator is calculated. Such models provide detail information about the structure of the cloud and cloud droplet spectra and were successfully compared with the aircraft observations (Leroy et al. 2009;Khairoutdinov and Kogan, 1999). These models

are used not only in a Large Eddy Simulation framework, but also in much larger scales, for instance to investigate effect of aerosol on hurricanes (Khain et al., 2009), as well as much smaller scales to investigate details of the cloud/clear air mixing processes (Andrejczuk et al., 2004). However, there are still unresolved issues in the bin approach, like how efficiently include information about aerosol, activation and/or deactivation of the aerosol or artificial spectrum broadening during condensational growth. Some of these issues are not present for 2 dimensional bin models, Clark (1973), Ovchinnikov and Easter (2010) which represent both aerosol and cloud droplet size, but such models are not in common use.

There are alternative numerical model approaches to the continuous droplet spectrum representation. Two models using Lagrangian approach to droplet/aerosol spectrum representation were developed recently - Lagrangian Cloud Model by Andrejczuk et al. (2008), later extended to include the collision-coalescence process Andrejczuk et al. (2010a) and a super-droplet approach by Shima et al. (2009). In this new formulation, Lagrangian parcels representing millions of physical aerosol particles are tracked within the Large Eddy Simulation (LES) model. Since each Lagrangian particle on each time step can be assigned to the grid of the LES model model, based on location, forces due to condensation/evaporation of the water on these parcels and drag forces can be evaluated, and returned to the LES model. Although these two models Andrejczuk et al. (2008, 2010a) and Shima et al. (2009) differ in details, they both represent the mixed Lagrangian-Eulerian approach, with the microphysical process represented in Lagrangian framework.

Since the Lagrangian representation of microphysics in LES models is new, validation is re-

quired to ensure that the model is capable of producing results qualitatively and/or quantitatively comparable with observations. Such an evaluation is the main focus of this paper, using the VOCALS observations to initialize and evaluate numerical model. This paper also shows the capability of the model to provide information about the relationship between aerosol and droplet properties inside a cloud that may help interpret aircraft observations or fill gaps in interpretation of these observations.

The next section discusses the numerical model, initial conditions and the model setup. Results are presented in section 3, followed by conclusions in section 4. The appendix discusses the model sensitivity to the number of parcels used in the simulations and the parameters the collision-coalescence algorithm depends on.

2. Numerical model

The numerical model representing microphysics in Lagrangian framework Andrejczuk et al. (2008, with the collision/coalescence process described in Andrejczuk et al. (2010a) is used to simulate a stratocumulus cloud. In this model microphysics formulated in a Lagrangian framework replaces the traditional Eulerian formulation and is coupled with the Eulerian dynamics and thermodynamics (Reisner et al., 2005). The Lagrangian microphysics tracks millions of parcels, each representing aerosol/droplets with the same chemical and physical (location in space, velocity) properties with the information about the dynamical and thermodynamical conditions provided by the Eulerian model. For each parcel, a full condensation model is solved and forces resulting from the phase change, together with the drag force are return to the Eulerian part of the model. Representation of the coalescence process in this framework calculates the collisions between each pair of a Lagrangian parcels within the collisional grid and creates new parcels. To limit the number of newly created parcels, a microphysical grid is used. Instead of creating a new parcel for each coalescence event, a new parcels are created for the microphysical grids for which number of assigned physical droplets is biggest than specified threshold level - T_L (4000 in the simulations reported in this paper, which corresponds to resolving 1 cloud droplet per m^3). This constraint is not sufficient, however, because new parcels are created at each time-step and with time, the number of parcels grows. An additional constraint, is to limit the number of parcels within each microphysical grid to 4. When there are more than 4 parcels in a microphysical grid, parcels are merged, with the merging procedure designed to conserve number of droplets and the masses of water and aerosol.

An important modification was introduced to the collision/coalescence to allow bigger time-steps between calls to collision procedure. When the time between collision calculations is too large, it can lead to a very small or even a negative number of cloud droplets existing parcel represents after the collisions with all other parcels within the collision grid. To avoid this problem, a threshold level T_L defining the minimum number of physical droplets within the Lagrangian parcel is also used to ensure that after a collision the number of physical droplets in the existing Lagrangian parcel is not less than this threshold level. Additional setp is added in the collision algorithm to verify how many droplets existing Lagrangian parcel would represent after the collision. If this number is less than the threshold level, all collisions with this parcel are recalculated using the modified number of droplets this parcel represents - $N_i^{'t}$:

$$N_i^{'t} = \frac{V_c}{\Delta t} \frac{T_L}{\sum_{j=1, j\neq i}^{P} K_{i,j} N_j^t}, \tag{1}$$

where V_c is the volume of the collision grid, Δt is time between collisions, T_L is a threshold level, $K_{i,j}$ - is the gravitational collision kernel, and j indexes the Lagangian parcels within the collision grid. After inserting this number into the equation describing cloud droplet number change after collisioni we have:

$$N_i^{t+1} = \frac{\Delta t}{V_c} N_i^{'t} \sum_{j=1//j\neq i}^{P} K_{i,j} N_j^t \tag{2}$$

that is, Lagrangian parcel i represents exactly T_L cloud droplets at time $t+1$.

In all the simulations reported in this paper, the described modifications were present. On some occasions this part of the algorithm was activated even in simulations calling the collision procedure every timestep. It produced negligible effect on solution. Because the collision algorithm has big impact on the execution time, calculation of the collision procedure with the time-step bigger than dt has advantages. However, as discussed in the appendix, modification to collision algorithms may also have significant impact on execution time when the time interval between calls to collision algorithm is too big.

3. Model setup and initial conditions

All the simulations reported here are in 2D. The domain covers 3200m in the horizontal and 2000m in vertical, and is resolved with the 80$\times$200 points. All the simulations were run for 7 hours with timestep 0.2s. For the first 2 hours the models were run without the collision process. The Eulerian microphysical grid for the collision mapping covers 1 - 500 μm in the cloud droplet radius space and 0.005 - 5 μm in the aerosol space and is resolved with 30$\times$30 grids.

To derive the initial conditions for the model, for each of the 3 discussed cases, a cloud penetration, long enough to supply information about the dynamical, thermodynamical, microphysical profiles and aerosol distribution through the boundary layer was chosen from the VOCALS observations (Wood et al., 2011). Three cases, refered as HIGH (profile from 13 Nov. 2008), MED (profile from 31 Oct. 2008) and LOW (profile from 13 Nov. 2008) were chosen based on the cloud droplet concentration measured inside the cloud. For all 3 cases profiles of potential temperature (θ) and water vapour mixing ratio (q_v) were specified as:

$$\theta(z) = \begin{cases} \theta_B, & z \leq z_B; \\ \theta_C + \alpha z, & z_B < z \leq z_T; \\ \theta_T + (z - z_T)^{2.8}, & z > z_T; \end{cases} \tag{3}$$

$$q_v(z) = \begin{cases} q_{vB} \text{ (or saturation)} & \text{if } z \leq z_T; \\ q_{vT} & \text{if } z > z_T; \end{cases} \tag{4}$$

with constants for each simulation defined in table 1.

Radiative forcing is based on the Stevens et al. (2005) parametrization. Only radiative cooling at the cloud top is taken into account and the longwave radiative flux is expressed as:

$$F_{rad} = F_0 exp^{-\kappa \int_z^\infty \rho q_c dz} \tag{5}$$

with $\kappa = 85m^2/kg$ and $F_0 = 35Wm^{-2}$.

For all cases the initial cloud water mixing ratio was specified, varying linearly with height inside the cloud, with the maximum value at the top of the boundary layer of $0.32[g/kg]$. The horizontal velocity (u component) was specified as height independent and was taken as the maximum of u and v from the observations: $1[m/s]$ for the HIGH run, $7[m/s]$ for the MED run and $4[m/s]$ for the LOW run. For all 3 cases the aerosol spectrum from SMPS (Scanning Mobility Particle Sizer) were analysed and a two modal log-normal distribution was fitted to the averaged aerosol

spectrum. For the HIGH and MED cases all observations from below the cloud within time specified in table 1 were used to calculate the parameters of the distributions. Averaged observations (x in figure 1), maximum and minimum values measured for each SMPS bin (dashed line) and a fitted log-normal distribution (solid line) for these 2 cases are shown in figure 1a and b. For the LOW case averaging all the observations below the cloud led to a distribution which for given forcing produced a much higher than observed cloud droplet concentration. Out of the 7 aerosol spectrum measurements only two, just below the cloud were taken into account when fitting log-normal distribution, with the resulting distribution shown in figure 1c. Parameters of a log-normal distribution for each of the cases are shown in table 2. Additionally log-normal distributions were fitted to the $mean$+/-σ and coefficients are also included in the table. For LOW case table 2 shows also coefficients for the whole below the cloud measurements including $mean$+/-σ.

Cases HIGH and MED are similar, with the observations taken in the region of unbroken cloud. Despite the fact that the flights were on different days, the height of the boundary level was about $\tilde{1}$400m for both cases, cloud is thicker for the HIGH case and is about 580 meters deep, compared to 400 meters for the MED. The biggest difference is in the cloud droplet concentration, with 250 cloud droplets cm^{-3} for the HIGH run and 120 cloud droplets cm^{-3} for the MED run. The LOW case is different. Although measurements were taken on the same day as for HIGH run, the boundary layer height is less than 1300 meters, cloud thickness is 360 meters and cloud droplet concentration is about 65 cm^{-3} The satellite image (e.g. Andrejczuk et al., 2010b figure 10) shows, that the region where measurements were taken is at the edge of the unbroken cloud with

the circulation changing from closed to open cells too west of this region.

In all the simulations 100 parcels per grid cell were used to represent the initial aerosol distribution, sresulting in 1.6 million parcels initially. As the model creates new parcels in the coalescence process the simulation HIGH, MED and LOW ended with 2.5, 2.3 and 2.2 million parcels respectively.

4. Results

4.1 General properties

Lagrangian representation of the microphysics provides information about the Lagrangian parcels locations and the sizes for each time step. This is shown in figure 2, after 7 hours, with each Lagrangian parcel with a radius bigger than 1 μm assigned to one of four classes with sizes [1-10] (red), [10-20] (green), [20-50] (blue), [50-100] (yellow) and bigger than 100 μm (magenta). Additionally contours of velocity are shown with solid line for positive and dashed line for negative values every 0.1 m/s, with contour 0 omitted. Figure 2 shows the complex structure of the flow and the parcels distribution in space. Typically the biggest drops (magenta) are located near the cloud base and centre and smallest droplets are distributed throughout the whole cloud. In some areas, in the up-draft, for the MED case, there is a clear transition from small to big droplet sizes (red->green->blue), but very often entrainment and falling droplets creates mixtures of the green and bluei; the range of sizes droplets can grow by condensation.

Since each parcel can represent a different number of cloud droplets/aerosol particles, with the biggest, created in collision process shaving the smallest number, the fact that parcels are present

in the model grid does not necessary mean that there is a significant amount of water in this grid. Combined information about size and number determines total mass of water in each grid. The cloud water mixing ratio diagnosed from the parcels size and location is presented in figure 3a-3c. Only values bigger than 0.05 g/kg are plotted with an interval of 0.1 g/kg. The cloud top reflects features shown in figure 2, since there are almost no parcels with radii bigger than 50 μm, created in the coalescence process and as a result representing much less cloud droplets than were initially assigned to each parcel. Near the cloud base, where such parcels are present, the contour of 0.05 g/kg is around 1000m for HIGH and MED and 800m for LOW. At the same time there are parcels present below these levels. These however, despite their big sizes, represent small number of cloud droplets and contribute little to q_c. Panels 3d-3f show mean profiles and standard deviations of q_c. The standard deviations of the cloud water mixing ratio are big, not only because of the variability due to dynamics, but also due to sampling error. The latter is a result of representing aerosol distribution with a limited number of parcels - 100 per grid initially. The transfer of one parcel from one grid to another represents a transfer of 1% of total the number of aerosol - leading to q_c variability since the same number of parcels in each grid can not be guaranteed.

The initial profiles and model solutions for potential temperature and water vapour mixing ratio are shown on figure 4 together with observed and modelled LWC (Liquid Water Content). The black lines show initial profiles derived from observations, and the grey lines show model output for the last 3 hours with the output saved every 6 minutes. For the LWC, observations rather than initial profiles are shown with each point representing one sample from the CDP (Cloud Droplet

Probe) probe. Both θ and q_v profiles show departure from initial values. The numerical model is unable to maintain sharp gradients near the top of the boundary layer, and below the cloud layer is cooling and drying with time.

Profiles of LWC - figure 4 show little change with time for all simulations, with the profiles for last 3 hours shown with the grey lines and observed profiles derived from the CDP measurement with x. Out of 3 cases considered in this paper the best agreement in LWC profiles soccur for LOW and MED simulations, with slightly deeper cloud produced by model for both runs. The HIGH simulation shows much bigger differences between model and observations especially near the cloud base. However, for MED and LOW cases, the LWC change with height is close to linear, whereas for HIGH case there is a change of slope near the cloud base, and may result from larger scale perturbation in the observations, not resolved by the model due to limited domain. Clearly, the model, when starting from an idealized q_c profile, is not able to reproduce this feature in the solution.

4.2 Microphysics

4.2.1 Cloud droplets

The cloud droplet number profiles measured by the CDP probe for each cloud section (x) and the corresponding model profiles are shown on figure 5. Although later the observations from CDP and 2DS (Two-Dimensional Stereo probe) are combined to produce cloud droplet spectrum, the droplet concentration from the 2DS probe for radii bigger than 25 μm was less than 2 cm^{-3} and these not included in figure 5. For the numerical model the cloud droplet concentration was

calculated based on the particle radius, with all particles with sizes bigger than 1 μm included. This method was used, instead of taking only cloud droplets having radius bigger than activation radius, because the CDP probe can not make distinction between cloud droplet and un-activated aerosol. In the numerical model, since full information about each parcel and thermodynamics is available such a distinction can be included and this is discussed later. For all 3 cases, the cloud droplet concentration changes little with height for both, simulations and observations. This suggests, that there is either a balance in droplet activation in downdrafts and deactivation in up-drafts, or droplets activate/deactivate near the cloud base only. The agreement in the cloud droplet concentration between the model solution and observations for all 3 runs is very good. Model profiles show the variability with time. This variability is, however, relatively small and are expected since the numerical solution is not in a steady state, but varies with time because the cloud may be at different stage of the development for each saved time. As for the LWC, cloud droplet number profiles indicate that model is producing a deeper cloud, for MED and LOW cases. For the MED case, the model also under-predicts cloud top height. For the HIGH run agreement between observations and model solution is not as good as for two other cases. As discussed earlier, the model does not capture the structure observed below 950 m., and under-predicts water content and cloud droplet number there, when starting from idealized profiles.

For the BAe-146 flights, the CDP and 2D-S were the only probes for which the droplet spectra were available. The CDP probe samples droplet with radius between 1 and 25 μm and thus provides mainly information about cloud droplets. The 2D-S provides information about droplet sizes

larger than 2.5 μm, but only sizes bigger than 25 μm were used for the analysis. Figure 6 displays the CDP measurements (with x), 2D-S measurements (with triangles) and model solution (each line represents one time with spectrum averaged over the whole domain for the last 3 hours) for passes through the cloud for the 3 cases considered in this paper. Only sizes smaller than 500 μm, the biggest bin size in the model, are shown. Spectra from the observations and from the model show good agreement for cloud droplets with radius r < 25 μm for HIGH and MED cases. For the LOW case agreement is not as good, but still reasonable. For sthe droplets larger than 25 μm (measured with 2D-S) the model under-predicts the droplet concentration for all 3 cases. Now, however, for the LOW case, the model solution is closest to the observations. Under-prediction of the biggest droplets concentration in the model indicates that coalescence process in the model is not efficient enough in production of big droplets. However it should be noted that there is a difference in the cloud droplet concentration for CDP and 2D-S for radius 25 μm, with the 2D-S measuring higher than CDP concentrations (especially for HIGH and MED). It may indicate that the 2D-S over-predicts the concentration of the big droplets or that the sample was not big enough to produce the right statistics. There is no consistent trend in the concentration of the largest drops. Both the observations and model show highest drop concentrations for the LOW case and lowest for the MED case.

Although averaged over the whole domain the spectra from the observations and the numerical model are similar, a detailed analysis shows that there are differences in droplet spectrum when comparing model - 7 hours into the simulation and the observed spectrum at a given level. The

droplet spectrum for 3 different heights in the cloud are shown in figure 7, with the top row showing spectrum near the the cloud top, the middle row showing spectrum in the middle of the cloud, and the bottom row showing spectrum near the cloud base for HIGH, MED and LOW runs. For the numerical model the spectrum on any given vertical level was horizontally averaged on this level for grids where $q_c > 0.001 g/kg$. From the observations the spectra at the height z_i were obtained by averaging the measurements in the vertical between $z_i - .5\Delta z$ and $z_i + .5\Delta z$, with $\Delta z = 10m$ - model grid size. Figure 7 shows that the model has problem with capturing details of the droplet spectrum on a given level. The differences between the model and the observations are present not only for the biggest droplets, created in the coalescence process, but also for the smallest. As the numerical model solution depends not only on microphysics, but also on the dynamics of the flow, this suggest that the dynamics of the solution may not be captured correctly perheps due to the lack of large scale forcing and the simulation being 2 dimensional. Note, however, that the observations were taken from only one penetration through the cloud for each case. Since the aircraft instrument samples only a small volume of the atmosphere, this disagreement may also indicate insufficient resolution of the observations.

The width of the droplet spectrum is an important factor affecting the coalescence process. Parcel models solved for the growth of an individual droplets tend to produce very narrow spectrum. Despite the fact that the condensation model used in the LCM is formulated in a Lagrangian framework, it does not produce narrow spectrum and the coalescence process is actively producing big cloud droplets. The latter has been shown already in figure 2 where big droplets are present

even for the run with a high aerosol concentration. Figure 8 shows profiles of the standard deviation (σ) of the cloud droplet distribution averaged over the last 3 hours of the simulation for the 3 cases considered in this paper, with the standard deviation showing values around 1.4 μm for HIGH, 1.1 μm for MED and 1.5 μm for LOW run, and varying with the height in the cloud. Only standard deviation smaller than 3 μm (5 μm for LOW run) are shown since near the cloud base fast evaporation for small droplets and slow for big droplets leads to significant growth of the standard deviation. Near the cloud top the increase of the standard deviation up to 3 μm is observed as a result of entrainment, mixing and subsequent evaporation. Aside from σ for the whole cloud, values for the up-draft and down-draft are also displayed. The general picture is similar for all runs, with σ in down-drafts bigger (as a result of droplet spectrum broadening during evaporation) than in up-drafts (droplet spectrum narrowing due to condensation). There is a tendency for an increase in σ in down-drafts near the cloud base as can be expected in the region of evaporation. No significant narrowing of the cloud droplet spectrum is observed in up-drafts (aside at the cloud base), contrary to parcel model predictions, where such a tendency is present [Bartlett and Jonas, 1972, Warner, 1969]. There are, however, significant differences between the microphysics in a parcel model and in the LCM model. In the LCM each parcel travels along different trajectory and encounters a different supersaturation history along the trajectory; dynamic and thermodynamic parameters are interpolated to the parcel location to determine the supersaturation for each parcel and as a result the effect of neighbouring grids and variability of the supersaturation inside the grid is taken into account; parcels do not move along air trajectories, with the velocity equations

solved for each parcel; and the coalescence process is very efficient in broadening the spectrum. Some of these processes and their effect on spectrum broadening were theoretically investigated by Cooper (1989) and Srivastava (1989) in the context of the turbulence and microscopic fluctuations in the supersaturation. Note, however, that in the model variability does not derive from these processes, but are purely a numerical effect because the dynamic/thermodynamic parameters are interpolated to the parcel location. The numerical model shows no consistent trend in σ behaviour for the whole cloud as a function of aerosol/cloud droplet concentration. It is biggest for the LOW and HIGH runs and smallest for MED run.

Additionally, figure 8 indicates the standard deviation of cloud droplet distribution derived from the CDP probe by means of trangles. Good agreement between the observations and the model is observed for HIGH and MED runs. For the LOW run the model under-predicts the standard deviation of the droplet spectrum inside the cloud by a factor of more than 2, with the 1.5 μm modelled and 3.3 μm observed. Few data points with the standard deviation smaller than the modelled values are also present in the observations for this case, indicating significant variability of the standard deviation in the observations. This difference between the model and the observations for the LOW case may be a result of the two dimensional domain. Andrejczuk et al. (2010a) shows a σ of almost 4 μm in 3D simulations using aerosol distribution observed during DYCOMS for very low aerosol concentrations.

4.2.2 Aerosol

Understanding the aerosol-cloud droplet relation is important not only for climate models, but

also for weather prediction models. Due to insufficient resolution, these models can not capture the variability within the cloud and as a result require parametrization of the relation between the aerosol concentration and the cloud droplet concentration. Results in this paper show that model with Lagrangian representation of microphysics gives a good agreement with observations not only for the cloud droplet number but also for the cloud droplet spectrum. In the coalescence process implementation, where 2 dimensional grid is used to map result of collision, both the aerosol radius and the cloud droplet radius is changing as a result of parcel collisions. With time, not only is the radius of the cloud droplets growing, but also the size of the aerosol inside this droplet. Figure 9 shows the aerosol spectrum inside the cloud, with initial aerosol spectrum (solid line), and spectra for the last 3 hours every 6 minutes (grey lines). For all casesi, the model is producing sizes larger than the initial distribution as a result of droplets coalescence, with the biggest aerosol radius about 2.3 μm for the HIGH and MED runs and 1.5 μm for the LOW run. For the LOW run, since the aerosol concentration is smallest and the droplet sizes biggest, one can expect to see larger maximum aerosol sizes than for the HIGH and MED runs. However one should appreciate that the biggest initial aerosol size was about 0.5 μm for the HIGH and MED and about 0.2 μm for the LOW case. It follows that the aerosol size grew almost 5 times in the HIGH and MED cases and almost 8 times in the LOW case. Production of the big aerosol particles in the collision process is rather slow and after 5 hours for the LOW run, only about 100 aerosol particles per m^3 with radius 1 μm is present inside the cloud.

Since the model gives detailed information about the aerosol and cloud droplets, it can be used

to produce a diagnostic relation about aerosol activation inside the cloud. Two lines are shown on each panel of the figure 10 with the averages over the last 1 hour taken to calculate the statistics. The solid line with x shows the percentage of activated aerosol - with a radius bigger than activation radius for each aerosol bin. For all cases the aerosol must be at least $0.02\mu m$ to be activated. The percentage of activated aerosol increases with the aerosol radius up to 90 % for the HIGH and MED run or 85 % for the LOW run and then decreases significantly. On the same plot a line with triangles shows the percentage of aerosol particles inside the droplets a with radius bigger than $1\mu m$ (both activated aerosol and aerosol with water on it but not exceeding the activation radius). This line shows a constant increase to 100 % reached for aerosol sizes of about $0.3\mu m$ for the HIGH and about $0.5\mu m$ for the MED and LOW cases, indicating that some of the droplets in the grids where cloud water is larger than $10^{-3}g/kg$ did not exceed activation radius. the location of the parcels with large aerosol inside (but not exceeding activation radius) show that these parcels reside not only at the edge of the cloud, but also inside the cloud and span the full spectrum of droplet sizes - from 1 to more than 100 μm. Having these parcels near the edge of the cloud is not surprising. Since each droplet sees the supersaturation at its location within the grid, at the edge of the cloud/clear air some of the droplets can evaporate and the radius can then drop below activation radius. Their presents inside the cloud may indicate an aerosol competing effect. Although for the big aerosol the activation supersaturation is small, the activation radius is big and as a result more time is needed for these particles to grow to the activation size (see Grabowski et al., 2011). Some of the droplets on big aerosol can not even grow by condensation to reach the activation radius,

since for aerosol of 1 μm, the activation radius is about 35 μm.

4.2.3 Relation between aerosol and cloud droplet sizes

In the model, full information about the aerosol and cloud droplet size is available. This data is presented on figure 11, where log_{10} of the droplet concentration is mapped on the collision grid for HIGH - panel a, MED - panel b and LOW - panel c cases. When integrated over the aerosol/droplet sizes the 2D cloud droplet concentration gives a cloud droplet spectrum or aerosol spectrum already discussed earlier in this paragraph. Figure 11 shows that the majority of the droplets are on aerosol particles with sizes .02 - .3 μm. A significant change is present for aerosol sizes about 0.01 μm with no aerosol particles having a significant amount of water below this size. Since the aerosol particles with sizes below 0.01 μm activate very quickly (the activation radius is very small), it indicates that the maximum supersaturation in the simulations does not exceed the critical supersaturation for this size. Indeed the maximum supersaturation, of the order of 1%, is observed at the end of the simulations, with a critical supersaturation for an aerosol radius 0.01 μm being more than 2%, at 283 K. The majority of the droplets on aerosol 0.02 - 0.3 μm have a size of less than 20 μm, indicating that condensation is the main process responsible for the droplet growth for these aerosol sizes. Aerosol particles with sizes larger than 0.3 μm are mainly inside the droplets with radius larger than 20 μm and these droplets are created in a collision process. For aerosol radii bigger than 0.3 μm, with increasing aerosol size the cloud droplet size also increases since more collision events are needed to create big droplets.

5 Summary and Conclusions

A Large Eddy Simulation model with a Lagrangian representation of microphysics is used to investigate the interactions between cloud, aerosol, dynamics and thermodynamics for a cloud topped boundary layer. The microphysics in Lagrangian formulations allow investigation of the cloud response to different aerosol concentrations and distributions, and provides detail information about aerosol-cloud droplet interactions. A distinct feature of this model is the treatment of the coalescence process on a 2 dimensional grid. As a result not only droplet sizes, but also aerosol sizes are processed in the coalescence process.

The numerical model captures general properties of the clouds, such as cloud droplet concentration and the profiles of cloud water, potential temperature and water vapour mixing ratio observed during the VOCALS field campaign; showing that it is possible to model the relation between the aerosol concentration and distribution and cloud droplet number for a stratocumulus cloud. For other features, such as the droplet spectrum (both averaged inside the cloud and on model levels), and the standard deviation of the cloud droplet distribution a difference between the observations and the model results are observed. The numerical model under-predicts the standard deviation of the cloud droplet distribution for run with low cloud droplet concentrations compared to observations (1.5 μm vs. 3.3 μm). The inability of the model to produce a bigger standard deviation of the cloud droplet distribution for low cloud droplet concentration run may be result of the 2D setup, since Andrejczuk et al., (2010a) 3D simulation for very low aerosol concentration produced standard deviation close to 4 μm.

The model results show that decreasing the cloud droplet/aerosol concentration doesn't lead

to a significant increase in either the largest cloud droplet sizes or the largest aerosol sizes. Since typically the biggest droplets have a big aerosol inside, one of the possible explanations is the removal of the big aerosol/droplets by drizzle.

This paper also shows the potential of the Lagrangian approach to microphysics to investigate cloud-aerosol interactions and provides examples of the information possible to be derived from such a model; for instance the size of the cloud droplets as a function of the aerosol size or the percentage of activated aerosol for different aerosol sizes. This information may be used in the future to help interpret aircraft observations or quantify the relation between the aerosol concentration and distribution and cloud droplet concentration and distribution. For each Lagrangian parcel the LCM model can distinguish between cloud droplets (having radius bigger than activation radius for given aerosol size) and aerosol with water (with radius smaller then activation radius). Model results show, that significant percentage of the droplets containing aerosol bigger than 0.3 does not exceed activation radius. As a result these can behave different than activated aerosol (with radius bigger than activation radius) and for instance with the decreasing supersaturation evaporate.

Appendix A: Sensitivity study As discussed and investigated in appendix of Andrejczuk et al. (2010a) the Lagrangina microphysics depends on a set of parameters. One of these parameters is the number of Lagrangian parcels used to represent the aerosol distribution in each model grid. In the simulations discussed here, 100 per model grid were used. For the MED casei, sensitivity runs were performed to investigate how the model solution depends on number of parcels. As well as 100 per grid, 50, 200 and 400 Lagrangian parcels were placed in each model grid. Figure 12 shows values averaged over the last 3 hours of bulk properties of the simulated cloud. There is variability in the model solution on changing the number of parcels, but there is no consistent trends. Figure 12a and 12d, the blue curve, indicates that using 50 parcels per model grid may not be enough, because both aerosol and droplet processing in the collision procedure leads to higher concentrations of the large aerosol and cloud droplets than for the other cases. The decrease of the standard deviation of the cloud water mixing ratio (σ_{q_c}) with the number of parcels used to represent initial aerosol distribution is small. This indicates that the variability shown in figure 3 is mainly due to dynamics. These are the only cases where consistent differences for runs with different number of parcels are observed. For other bulk properties, the differences are either small or show no trends indicating that the variability in bulk cloud properties shown in figure 12 is a result of the different referred of the solutions resulting from the different forcing and interactions between microphysics and dynamics/thermodymanics.

The other parameters solution depend are: a threshold level (T_l) defining minimum number of cloud droplets that the Lagrangian parcel represents, whether model grid is split into collision

grids and how many parcels are allowed in one bin before parcels are merged. Sensitivity of the solution to these parameters is shown in figure 13a-13d. Decreasing T_l, not splitting model grid into 4 collision grids, and merging parcels when the difference in size is less than the quarter of the bin size (half of the bin size in reference MED run) has a similar effect and leads to bigger drizzle sizes, higher drizzle concentrations and a larger concentration of the aerosol created in coalescence process compared to MED reference run. Despite the differences in the cloud droplet and aerosol distributions cloud water and cloud droplet number profiles are very similar.

Panels e-h of the figure 13 show the sensitivity of the solution to the frequency of the calls to collision procedure. Beside the reference run, where the call is every time step two additional runs were performed, one with the call every 5 timesteps (1 s) and one with the call every 150 timesteps (300 s). Solution with the calls every 1s is very similar to the reference solution, and the difference between these two solutions is within the variability for the solutions discussed already. Solution with the call to the collision routine every 300 s produced much smaller drizzle sizes, but with higher than the reference (MED) drizzle concentrations and also processed almost no aerosol. Additionally there is almost no speed-up (1%) of the model execution when the collision procedure was called every 300 s, compared to 15% speed-up for the run with calls every 1 s. This indicates that the additional part of the collision algorithm responsible for keeping number of physical droplets in each Lagrangian parcel above threshold level has a significant effect on execution time. It follows that rather moderate time between calls to collision routine may be used to obtain faster model execution.

In the LCM the droplet growth is grid free, but the microphysical grid is required to map collisions. As a result the solution depends on the number of bins used to represent the aerosol and the cloud droplet radius space. Results of the simulations shown in figure 14a - 14d show little sensitivity of the solution with different number of bins (10, 30 and 60) used to represent aerosol sizes, when number of bins used to represent droplet spectrum is 30. The model is much more sensitive to the number of bins used to represent droplet spectrum for 30 aerosol bins (14e - 14h); where with a increasing number of bins, the concentration and biggest drizzle sizes increases. The model also processes the aerosol more efficiently with an increasing number of droplet bins, as indicated by the increase of aerosol concentration for sizes bigger than 1 μm. The changes in the mean q_c profiles are small, but use of the 60 bins to represent droplet sizes decreases cloud droplet number concentration. Although increasing number of bins tends to improve the solution (simulations using 30 bins under-predict drizzle concentrations compared to observations) it comes with an increase of CPU time and model execution with 60 bins used to represent droplet sizes is almost two times more expensive (increase by 90%) than the run with 30 bins.

Acknowledgements. This work was supported by NERC grant NE/F018673/1. Observational data was provided by the British Atmospheric Data Centre (BADC). The authors would like to thank Dr Ian Crawford, Dr Jonathan Crosier and Dr Grant Allen from Manchester University for providing aerosol and microphysical data. The authors thank dr. Wojciech Grabowski for his comments. This work made use of the facilities of HECToR, the UK's national high-performance computing

service, which is provided by UoE HPCx Ltd at the University of Edinburgh, Cray Inc and NAG Ltd, and funded by the Office of Science and Technology through EPSRC's High End Computing Programme.

References

Ackerman, A., M. P. Kirkpatrick, D. E. Stevens, and O. B. Toon: 2004, The impact of humidity above stratiform clouds on indirect aerosol climate forcing. *Nature*, **342**, 1014–1017.

Andrejczuk, M., W. Grabowski, J. Reisner, and A. Gadian: 2010a, Cloud-aerosol interactions for boundary-layer stratocumulus in the lagrangian cloud model. *J. Geophys. Res.*, **115**, D22214, doi:10.1029/2010JD014248.

Andrejczuk, M., W. W. Grabowski, A. Gadian, and R. Burton: 2010b, Limited-area modelling of stratocumulus over south-eastern pacific. *Atmos. Chem. Phys. Discuss.*, **11**, 25517–25556, doi:10.5194/acpd–11–25517–2011.

Andrejczuk, M., W. W. Grabowski, S. P. Malinowski, and P. K. Smolarkiewicz: 2004, Numerical simulation of cloud-clear air interfacial mixing. *J. Atmos. Sci.*, **61**, 1726–1739.

Andrejczuk, M., J. M. Reisner, B. F. Henson, M. Dubey, and C. A. Jeffery: 2008, The potential impacts of pollution on a nondrizzling stratus deck: Does aerosol number matter more than type? *J. Geophys. Res.*, **113**, D19204, doi:10.1029/2007JD009445.

Bartlett, J. . T. and P. R. Jonas: 1972, On the dispersion of the sizes of droplets growing by condensation in turbulent clouds. *Quart. J. Roy. Meteor. Soc.*, **98**, 150–164.

Clark, T.: 1973, Numerical modeling of the dynamics and microphysics of warm cumulus convection. *J. Atmos. Sci.*, **30**, 857–878.

Cooper, W. A.: 1989, Effects of variable droplet growth histories on droplet size distributions. part I: Theory. *J. Atmos. Sci.*, **46**, 1301–1311.

Ferrier, B. S.: 1994, A double-moment multiple-phase four-class bulk ice scheme. part I: Description. *J. Atmos. Sci.*, **51**, 249–280.

Grabowski, W. W., M. Andrejczuk, and L.-P. Wang: 2011, Droplet growth in a bin warm-rain scheme with twomey ccn activation. *Atmos. Res.*, **99**, 290–301.

Kessler, E.: 1969, On the distribution and continuity of water substance in atmospheric circulations. *Meteor. Monogr.*, **32**.

Khain, A., B. Lynn, and J. Dudhia: 2009, Aerosol effects on intensity of landfalling hurricanes as seen from simulations with the wrf model with spectral bin microphysics. *J. Atmos. Sci.*, **67**, 365–384.

Khain, A. P., A. Pokrovsky, M. Pinsky, A. Seifert, and V. Phillips: 2004, Simulation of effects of atmospheric aerosols on deep turbulent convective clouds using a spectral microphysics mixed-phase cumulus cloud model. part i: Model description and possible applications. *J. Atmos. Sci.*, **61**, 2963–2982.

Khairoutdinov, M. and Y. Kogan: 2000, A new cloud physics parameterization in a large-eddy simulation model of marine stratocumulus. *Mon. Wea. Rev.*, **128**, 229–243.

Khairoutdinov, M. F. and Y. L. Kogan: 1999, A large eddy simulation model with explicit micro-

physics: Validation against aircraft observations of a stratocumulus-topped boundary layer. *J. Atmos. Sci.*, **56**, 2115–2131.

Koenig, L. R. and F. W. Murray: 1976, Ice-bearing cumulus cloud evolution: Numerical simulation and general comparison against observations. *J. Appl. Meteor.*, **15**, 747–762.

Leroy, D., W. Wobrock, and A. I. Flossmann: 2009, The role of boundary layer aerosol particles for the development of deep convective clouds: A high-resolution 3d model with detailed (bin) microphysics applied to crystal-face. *Atmos. Res.*, **91**, 62–78.

Meyers, M. P., R. L. Walko, J. Y. Harrington, and W. R. Cotton: 1997, New rams cloud microphysics parameterization. part II: The two-moment scheme. *Atmos. Res.*, **45**, 3–39.

Milbrandt, J. A. and M. K. Yau: 2005, A multimoment bulk microphysics parameterization. part I: Analysis of the role of the spectral shape parameter. *J. Atmos. Sci.*, **62**, 3051–3064.

Morrison, H., J. A. Curry, and V. I. Khvorostyanov: 2005, A new double-moment microphysics parameterization for application in cloud and climate models. part I: Description. *J. Atmos. Sci.*, **62**, 1665–1677.

Ovchinnikov, M. and R. C. Easter: 2010, Modeling aerosol growth by aqueous chemistry in a non-precipitating stratiform cloud. *J. Geophys. Res.*.

Reisner, J. M., V. Mousseau, A. Wyszogrodzki, and D. Knoll: 2005, A fully implicit hurricane model with physics-based preconditioning. *Mon. Wea. Rev.*, **133**, 1003–1022.

Seifert, A. and K. D. Beheng: 2001, A double-moment parameterization for simulating autoconversion, accretion and self-collection. *Atmos. Res.*, **59-60**, 265–281.

Shima, S., K. Kusano, A. Kawano, T. Sugiyama, and S. Kawahara: 2009, The super-droplet method for the numerical simulation of clouds and precipitation: a particle-based and probabilistic microphysics model coupled with a non-hydrostatic model. *Quart. J. Roy. Meteor. Soc.*, **135**, 1307–1320.

Srivastava, R. C.: 1989, Growth of cloud drops by condensation: A criticism of currently accepted theory and a new approach. *J. Atmos. Sci.*, **46**, 869–887.

Stevens, B., C.-H. Moeng, A. S. Ackerman, C. S. Bretherton, A. Chlond, S. de Roode, J. Edwards, J.-C. Golaz, H. Jiang, M. Khairoutdinov, M. P. Kirkpatrick, D. C. Lewellen, A. Lock, F. Mller, D. E. Stevens, E. Whelan, and P. Zhu: 2005, Evaluation of large-eddy simulations via observations of nocturnal marine stratocumulus. *Mon. Wea. Rev.*, **133**, 1443–1462.

Warner, J.: 1969, The microstructure of cumulus cloud. part II. the effect on droplet size distribution of cloud nucleus spectrum and updraft velocity. *Quart. J. Roy. Meteor. Soc.*, **26**, 1272–1282.

Wood, R., C. R. Mechoso, C. S. Bretherton, and coauthors: 2011, The vamos ocean-cloud-atmosphere-land study regional experiment (VOCALS-REx): Goals, platforms and field operations. *Atmos. Chem. Phys. Discuss.*, **11**, 627–654.

List of Tables

1 Constants used to define profiles of the potential temperature, water vapour mixing ratio and cloud water mixing ratio. 32

2 Parameters of log-normal distributions observed/used in simulations. σ_+, σ_- are fits for the observed $mean$+/-σ. LOW specifies aerosol distribution used in simulations (averaged for only 2 measurements). LOWA is the mean for all below the cloud observations with the corresponding fits for observations +/-σ given by σ_+/σ_-. 33

Table 1: Constants used to define profiles of the potential temperature, water vapour mixing ratio and cloud water mixing ratio.

RUN	z_B [m]	z_T [m]	θ_B [K]	θ_C [K]	θ_T [K]	q_{vB} [g/kg]	q_{vT} [g/kg]	α [K/m]	Observation time [UTC]	Date
HIGH	800	1380	291.1	288.5	302.5	8.3	0.3	3.3×10^{-3}	11.08-11.28	13 Nov. 2008
MED	1000	1400	289.2	286.2	299.0	7.0	0.7	3.0×10^{-3}	11.36-12.03	31 Oct. 2008
LOW	900	1260	290.1	287.6	301.0	7.8	0.7	2.7×10^{-3}	11.47-12.02	13 Nov. 2008

Table 2: Parameters of log-normal distributions observed/used in simulations. σ_+, σ_- are fits for the observed $mean$+/-σ. LOW specifies aerosol distribution used in simulations (averaged for only 2 measurements). LOWA is the mean for all below the cloud observations with the corresponding fits for observations +/-σ given by σ_+/σ_-.

RUN		$N_1[cm^{-3}]$	$r_1[\mu m]$	σ_1	$N_2[cm^{-3}]$	$r_2[\mu m]$	σ_2
HIGH		380	0.071	0.45	160	0.029	0.31
	σ_+	448	0.074	0.42	227	0.031	0.33
	σ_-	327	0.064	0.53	78	0.027	0.27
MED		118	0.10	0.43	129	0.022	0.36
	σ_+	212	0.10	0.56	151	0.022	0.31
	σ_-	47	0.10	0.28	89	0.022	0.39
LOW		42	0.11	0.25	111	0.023	0.47
LOWA		63	0.10	0.27	134	0.025	0.50
	σ_+	84	0.10	0.28	170	0.025	0.54
	σ_-	41	0.10	0.24	99	0.025	0.45

List of Figures

1 Averaged measured (x), fitted(solid line) and maximum/minimum measured (dashed line) of aerosol distribution for HIGH (a), MED (b) and LOW (c) cases. 38

2 Locations and sizes of Lagrangian parcels after 7th hour of simulations; run HIGH - panel a, run MED - panel b, run LOW - panel c. Red colour parcel sizes 1-10 μm, green - 10-20 μm, blue 20-50 μm, yellow 50-100 μm, and magenta - bigger than 100 μm. 39

3 Panels a-c cloud water mixing ratio diagnosed from Lagrangian parcels location and size after 7 hours of simulations. Panels d-f - cloud water mixing ratio profile (solid line), with standard deviation (dashed lines). 40

4 Initial profiles of θ and q_v - black line and model solution for HIGH run (a and b), MED run (d and e) and LOW run (g and h) - grey lines. Panels c, f, i - LWC profiles derived from model (grey lines; last 3 hours) with observations (CDP probe) - x. . 41

5 Profiles of cloud droplet number as measured by CDP probe (x) and modelled (grey lines; last 3 hours) for runs HIGH (a), MED (b), LOW (c). 42

6 Cloud droplet spectrum averaged over the whole domain. CDP probe (x), 2D-S probe triangles and from model grey lines (last 3 hours). 43

7 Cloud droplet spectrum for different locations inside the cloud. Top row - near the cloud top, middle row - near cloud center, low row - near the cloud base for HIGH (left column), MED (middle column) and LOW (right column). Solid line - model, symbols - CDP (x) and 2D-S (triangles) 44

8 Profiles of the standard deviation of the cloud droplet distribution, measured by CDP probe (x) and modelled - lines. Solid line - whole cloud, dotted line up-drafts only, dashed line down-drafts only. Run HIGH - panel a, run MED - panel b and run LOW - panel c 45

9 Evolution of the aerosol distribution for the last 3 hours (grey lines) and initial aerosol distribution black line with 'x' for run HIGH - panel a, MED - panel b and LOW - panel c. 46

10 Percentage of droplets with radius bigger than the activation radius (stars), and with droplet size bigger than 1 μm - both activated and not activated (triangles) as a function of aerosol radius for run HIGH - panel a, MED - panel b and LOW - panel c. Averages over the last 1 hour were taken to calculate the statistics. 47

11 $Log_{10}(N_d)$ as a function of aerosol and cloud droplet radius, for run HIGH - panel a, run MED - panel b, and run LOW - panel c. 48

12 Sensitivity of the model solution for MED aerosol distribution to the number of parcels used to represent initial aerosol distribution: 50 - blue, 100 - black, 200 - green, 400 - red. Panel a - droplet spectrum, panel b - cloud water mixing ratio profile, panel c - cloud droplet number profile, panel d - aerosol spectrum, panel d - profile of the standard deviation of the cloud water mixing ratio, panel e - profile of the standard deviation of the cloud droplet spectrum. All profiles are averaged over the last 3 hours. 49

13 Left panels - mean profiles for the simulations: MED - black (T_l=4000, computational grid split into 4 collision grids, parcels merged when difference in size is less than half of the bin width), simulation with T_l = 1 - blue, simulation with the collision grid the same as computational grid - red, simulation when parcels are merged for the difference in size less than a quarter of the bin width - green. Right panels - mean profiles for the simulations: MED - black (collision called every time step), collision called every 5 time steps (1s) - blue, collision called every 150 time steps (30s) - green. All profiles are averaged over the last 3 hours. Panels a/e droplet spectrum, panels b/f - aerosol spectrum, panels c/g cloud water mixing ration profile, panels d/h - cloud droplet number profiles. 50

14 Left panels - mean profiles for the simulations with 30 droplet radius bins and 10 - blue, 30 (MED run) - black, and 60 - green, aerosol bins. Right panel - mean profiles for the simulations with 30 aerosol radius bins and 10 - blue, 30 (MED run) - black, and 60 - green, droplet radius bins. All profiles are averaged over the last 3 hours. Panels a/e droplet spectrum, panels b/f - aerosol spectrum, panels c/g cloud water mixing ration profile, panels d/h - cloud droplet number profiles. . . . 51

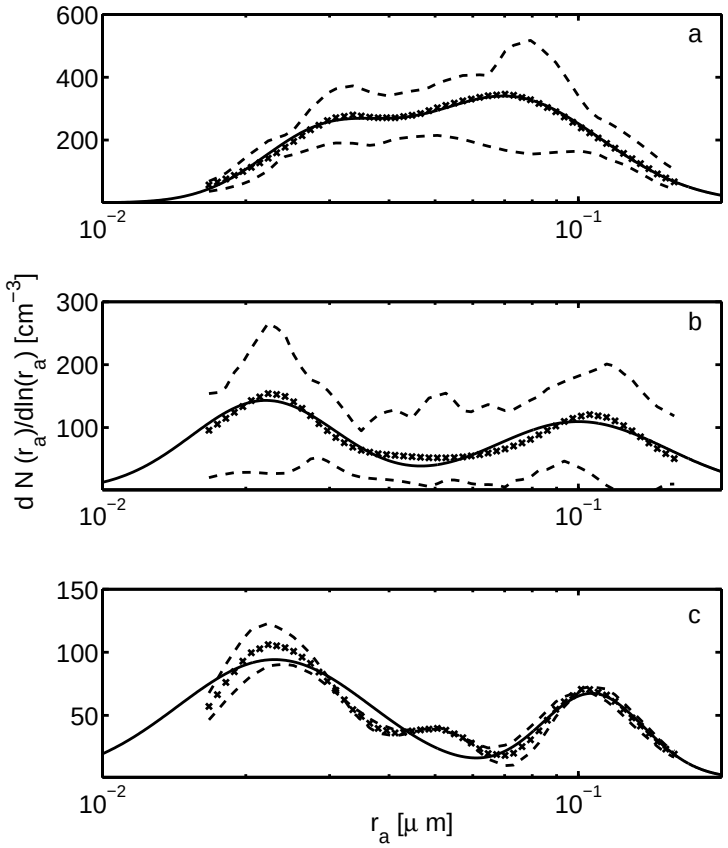

Figure 1: Averaged measured (x), fitted(solid line) and maximum/minimum measured (dashed line) of aerosol distribution for HIGH (a), MED (b) and LOW (c) cases.

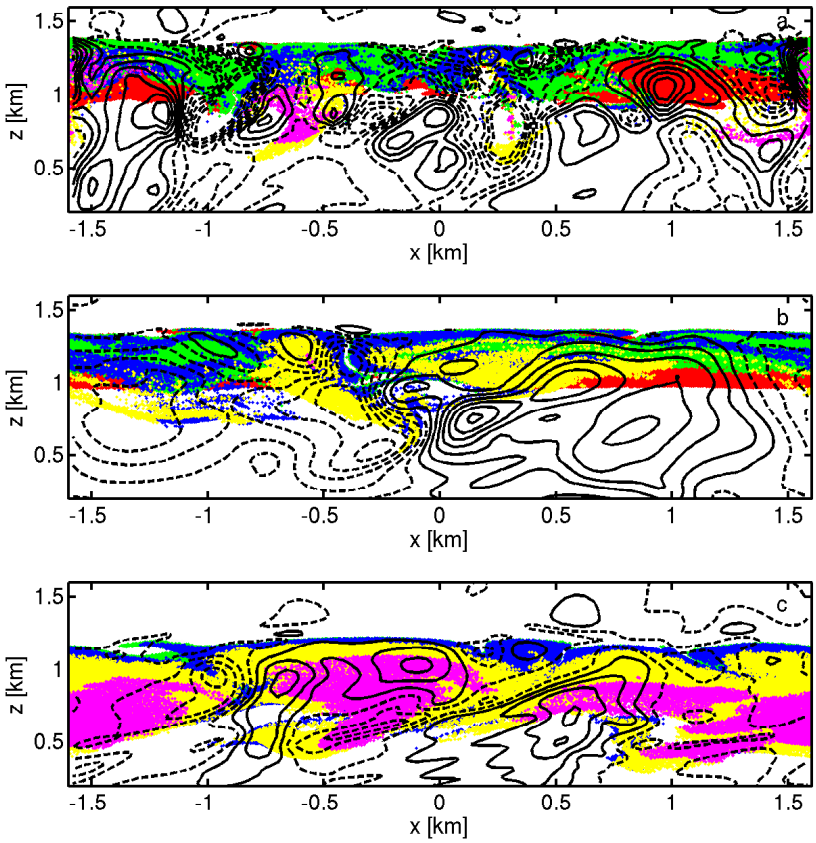

Figure 2: Locations and sizes of Lagrangian parcels after 7th hour of simulations; run HIGH - panel a, run MED - panel b, run LOW - panel c. Red colour parcel sizes 1-10 μm, green - 10-20 μm, blue 20-50 μm, yellow 50-100 μm, and magenta - bigger than 100 μm.

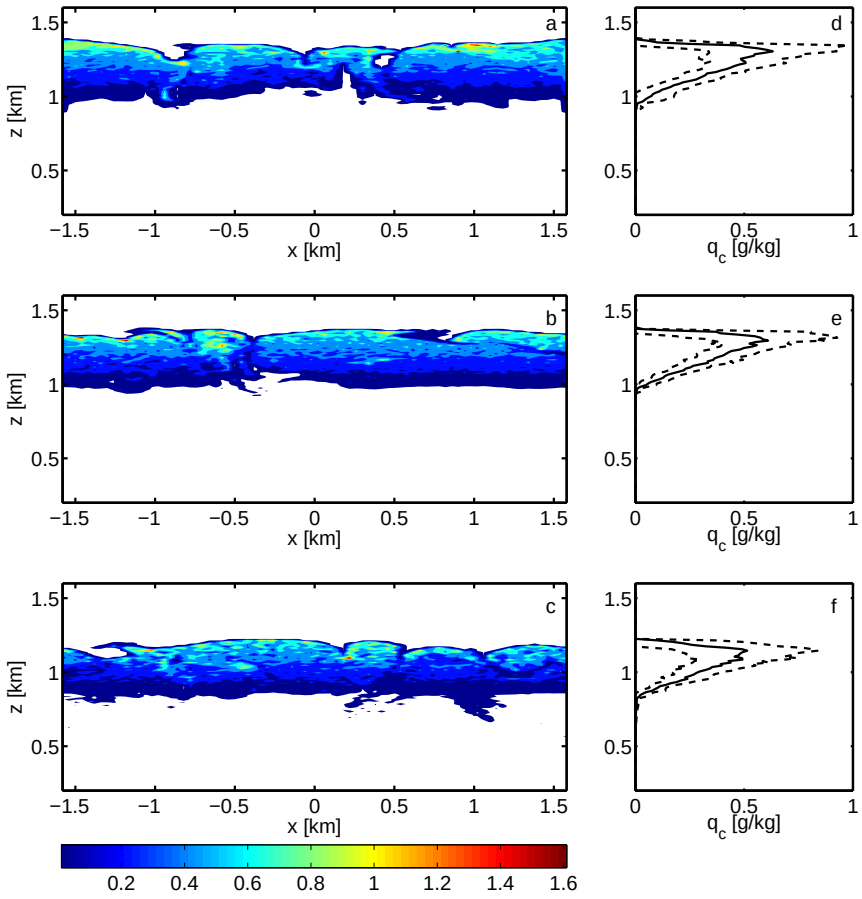

Figure 3: Panels a-c cloud water mixing ratio diagnosed from Lagrangian parcels location and size after 7 hours of simulations. Panels d-f - cloud water mixing ratio profile (solid line), with standard deviation (dashed lines).

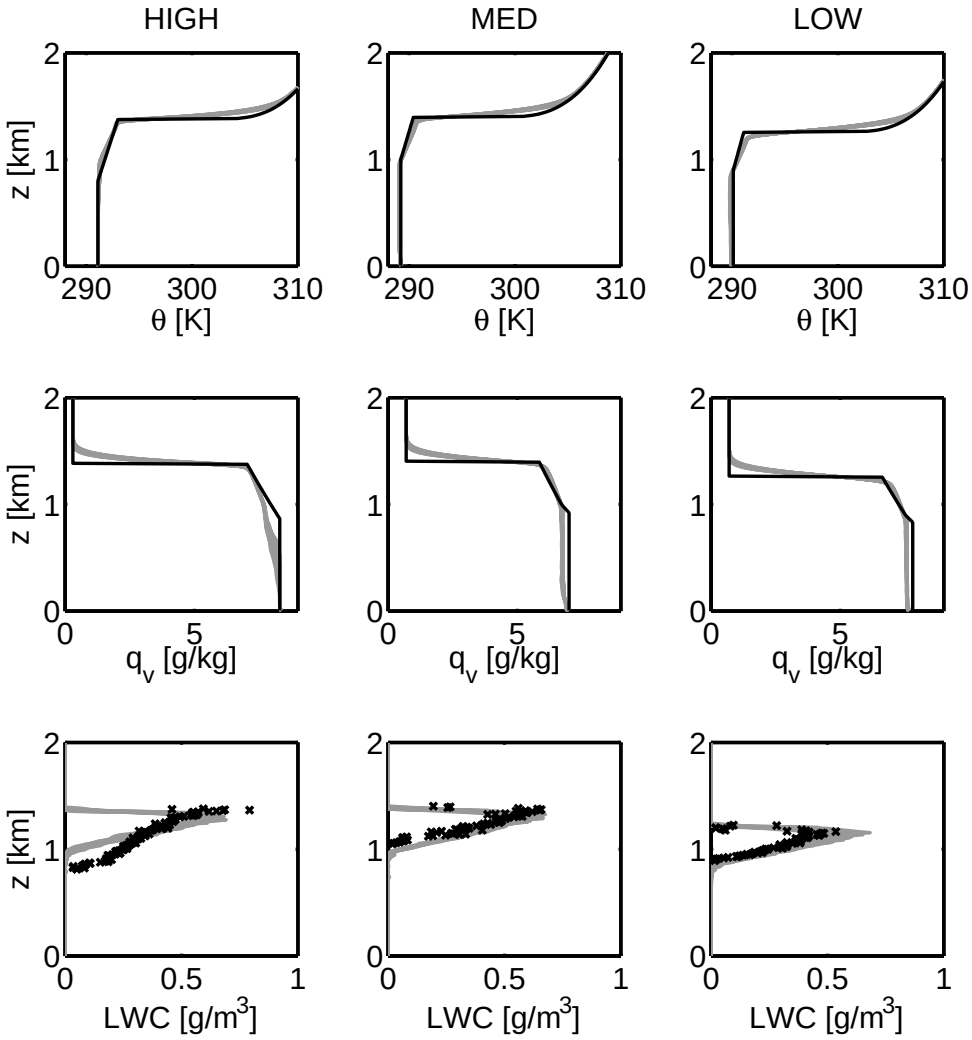

Figure 4: Initial profiles of θ and q_v - black line and model solution for HIGH run (a and b), MED run (d and e) and LOW run (g and h) - grey lines. Panels c, f, i - LWC profiles derived from model (grey lines; last 3 hours) with observations (CDP probe) - x.

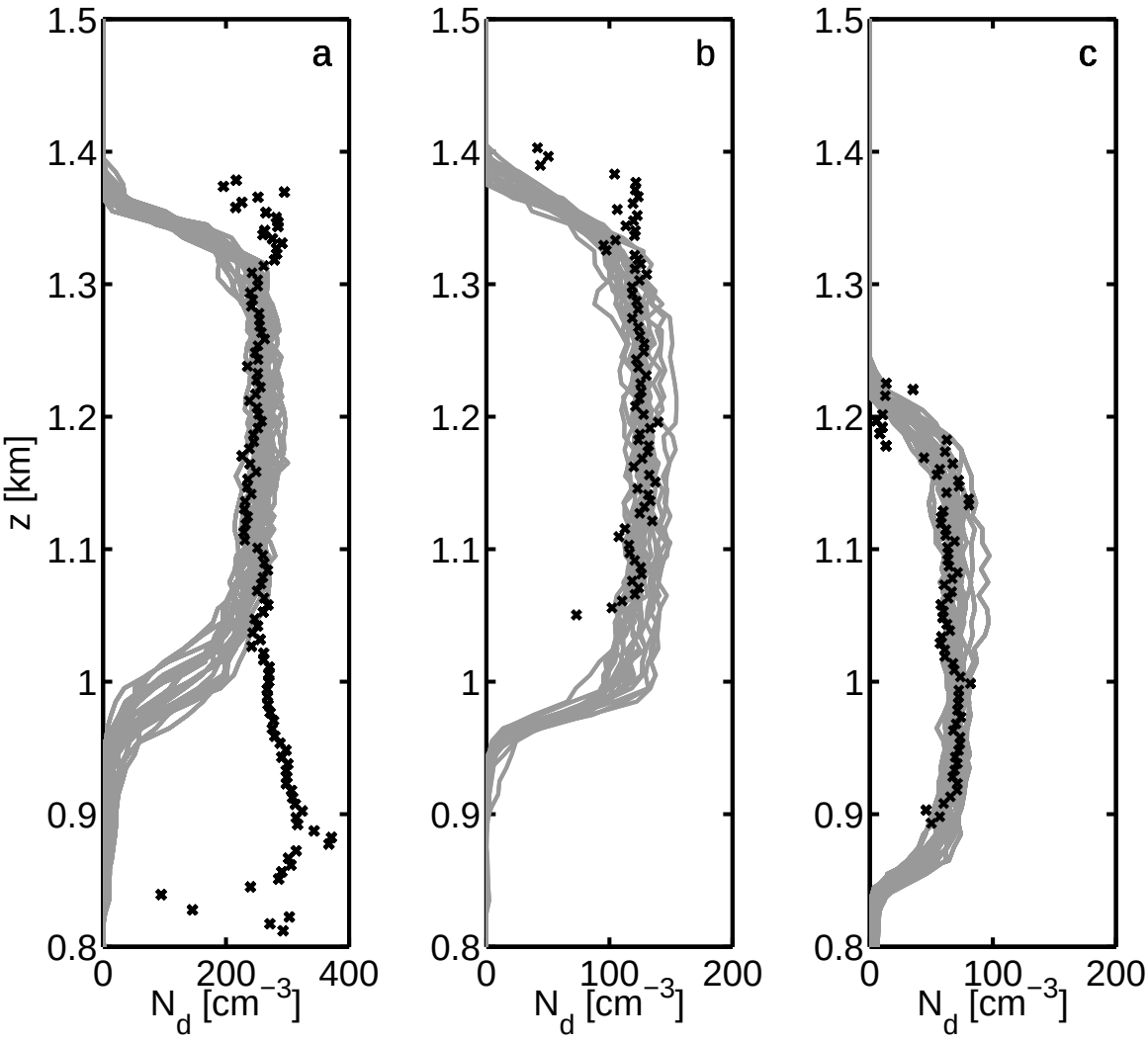

Figure 5: Profiles of cloud droplet number as measured by CDP probe (x) and modelled (grey lines; last 3 hours) for runs HIGH (a), MED (b), LOW (c).

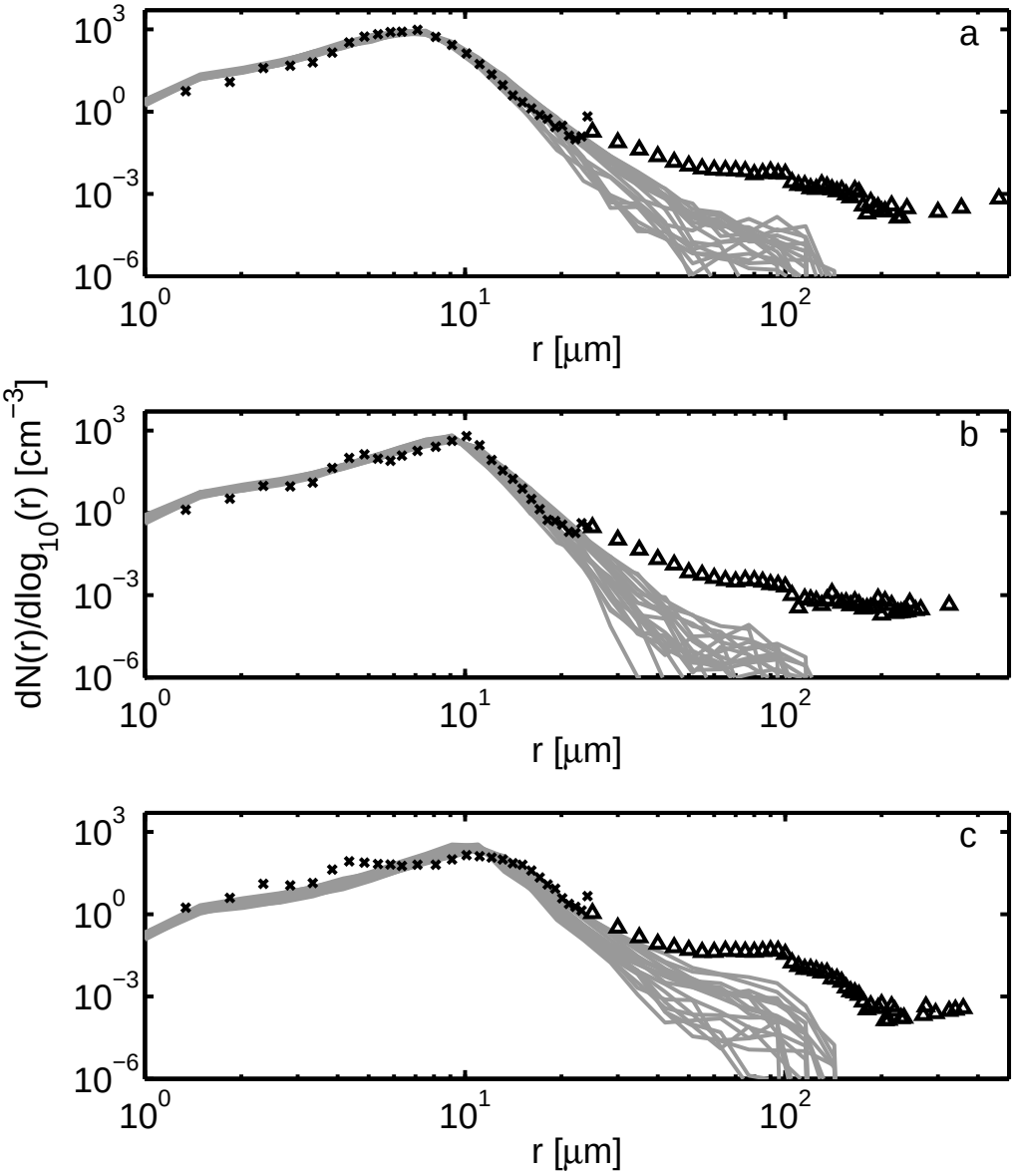

Figure 6: Cloud droplet spectrum averaged over the whole domain. CDP probe (x), 2D-S probe triangles and from model grey lines (last 3 hours).

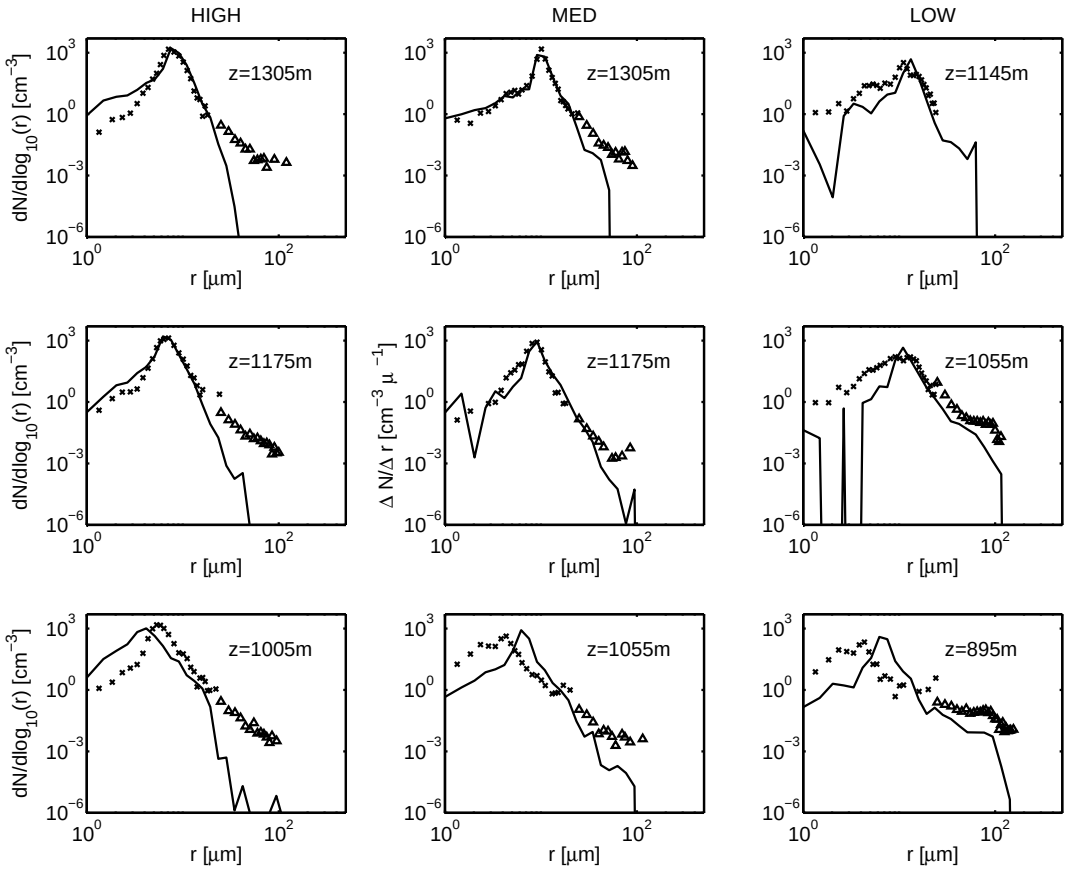

Figure 7: Cloud droplet spectrum for different locations inside the cloud. Top row - near the cloud top, middle row - near cloud center, low row - near the cloud base for HIGH (left column), MED (middle column) and LOW (right column). Solid line - model, symbols - CDP (x) and 2D-S (triangles)

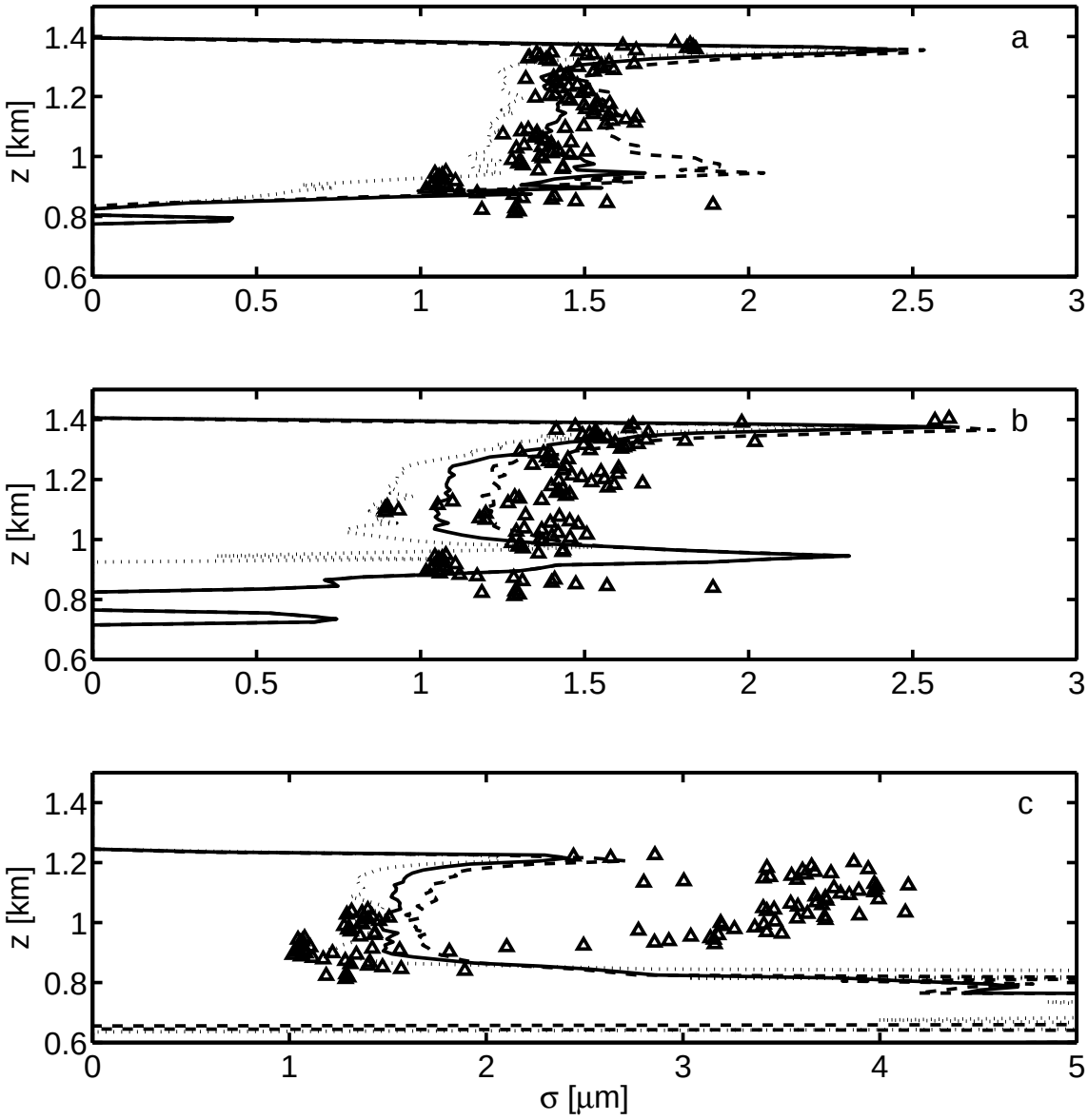

Figure 8: Profiles of the standard deviation of the cloud droplet distribution, measured by CDP probe (x) and modelled - lines. Solid line - whole cloud, dotted line up-drafts only, dashed line down-drafts only. Run HIGH - panel a, run MED - panel b and run LOW - panel c

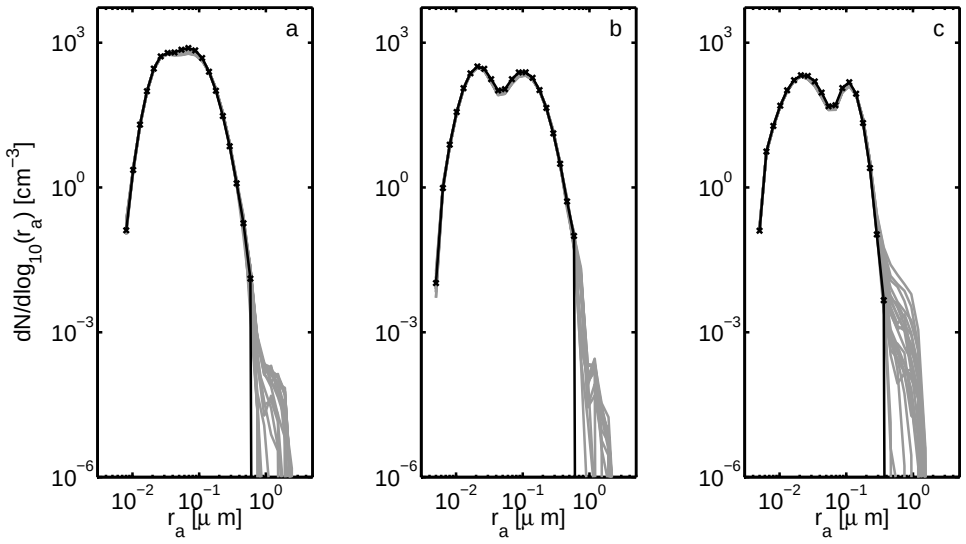

Figure 9: Evolution of the aerosol distribution for the last 3 hours (grey lines) and initial aerosol distribution black line with 'x' for run HIGH - panel a, MED - panel b and LOW - panel c.

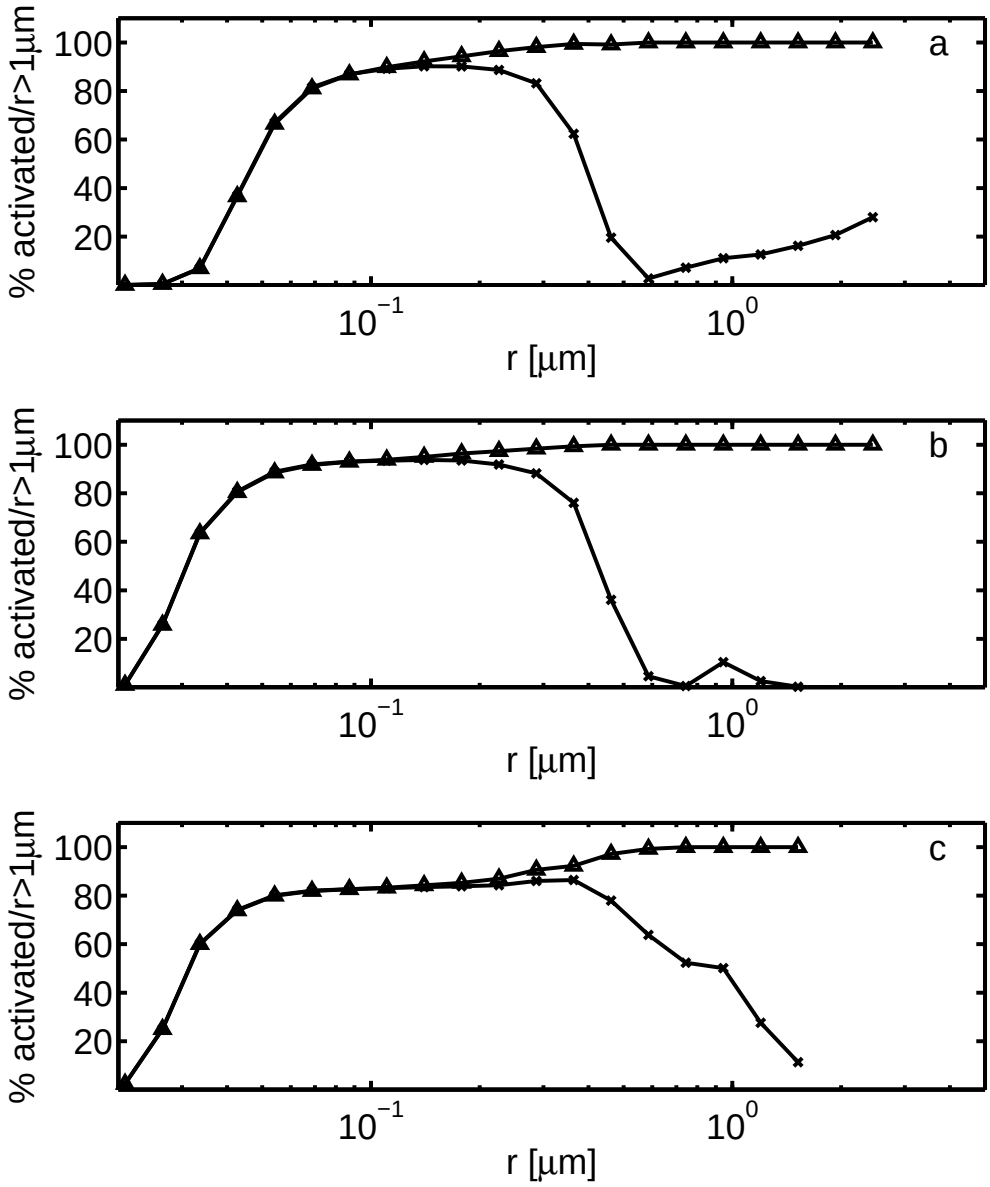

Figure 10: Percentage of droplets with radius bigger than the activation radius (stars), and with droplet size bigger than 1 μm - both activated and not activated (triangles) as a function of aerosol radius for run HIGH - panel a, MED - panel b and LOW - panel c. Averages over the last 1 hour were taken to calculate the statistics.

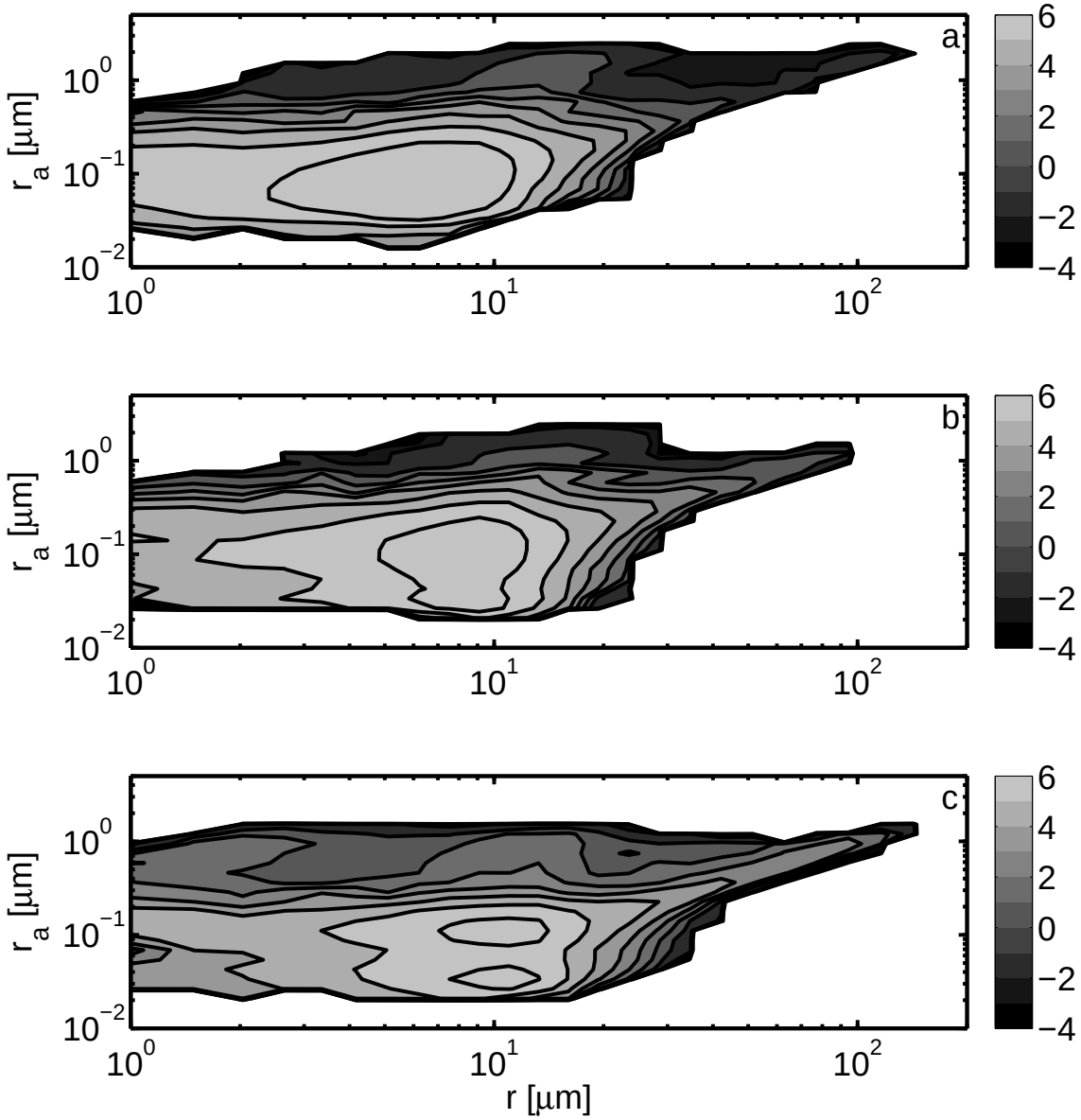

Figure 11: $Log_{10}(N_d)$ as a function of aerosol and cloud droplet radius, for run HIGH - panel a, run MED - panel b, and run LOW - panel c.

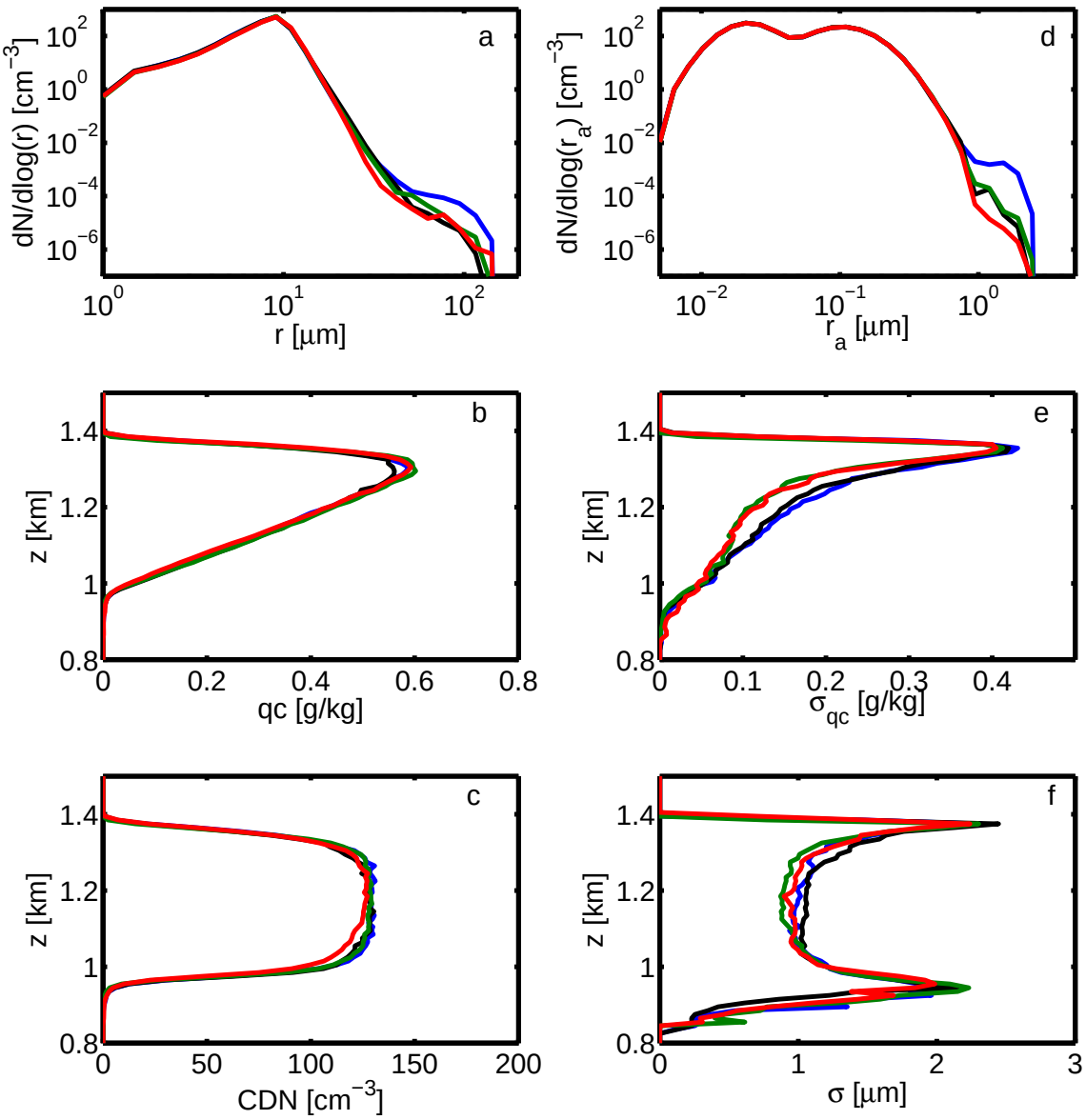

Figure 12: Sensitivity of the model solution for MED aerosol distribution to the number of parcels used to represent initial aerosol distribution: 50 - blue, 100 - black, 200 - green, 400 - red. Panel a - droplet spectrum, panel b - cloud water mixing ratio profile, panel c - cloud droplet number profile, panel d - aerosol spectrum, panel d - profile of the standard deviation of the cloud water mixing ratio, panel e - profile of the standard deviation of the cloud droplet spectrum. All profiles are averaged over the last 3 hours.

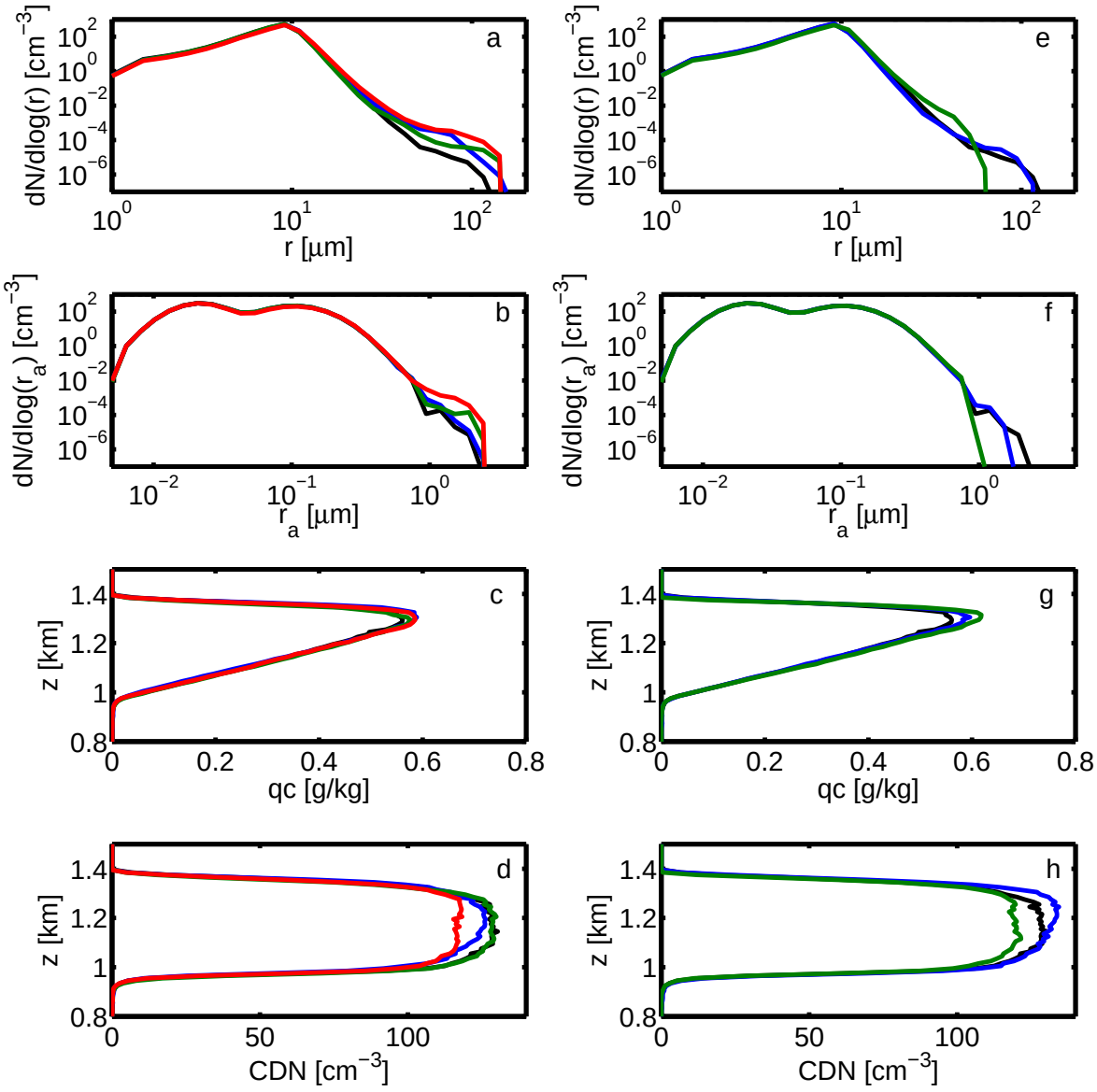

Figure 13: Left panels - mean profiles for the simulations: MED - black (T_l=4000, computational grid split into 4 collision grids, parcels merged when difference in size is less than half of the bin width), simulation with T_l = 1 - blue, simulation with the collision grid the same as computational grid - red, simulation when parcels are merged for the difference in size less than a quarter of the bin width - green. Right panels - mean profiles for the simulations: MED - black (collision called every time step), collision called every 5 time steps (1s) - blue, collision called every 150 time steps (30s) - green. All profiles are averaged over the last 3 hours. Panels a/e droplet spectrum, panels b/f - aerosol spectrum, panels c/g cloud water mixing ration profile, panels d/h - cloud droplet number profiles.

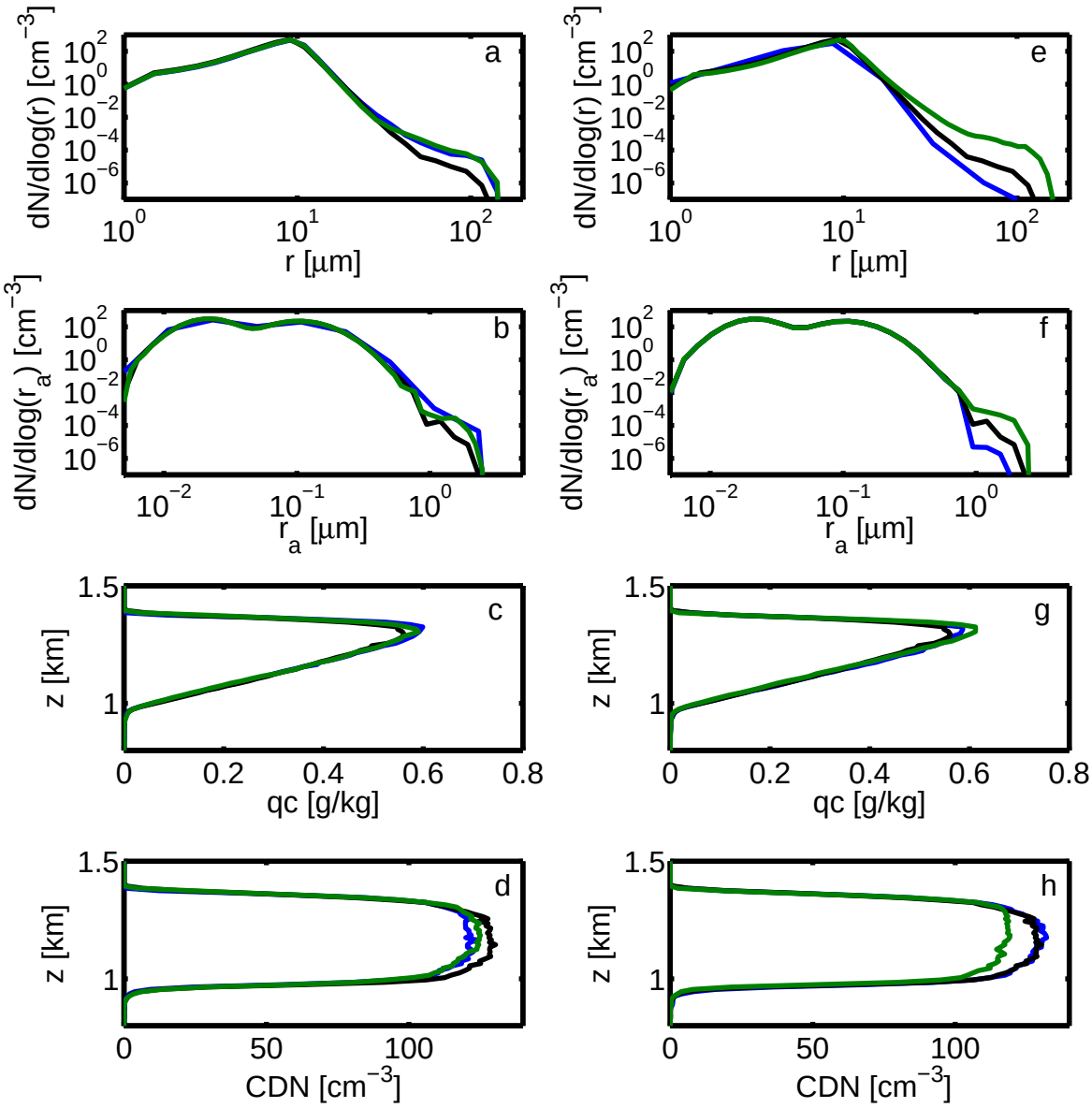

Figure 14: Left panels - mean profiles for the simulations with 30 droplet radius bins and 10 - blue, 30 (MED run) - black, and 60 - green, aerosol bins. Right panel - mean profiles for the simulations with 30 aerosol radius bins and 10 - blue, 30 (MED run) - black, and 60 - green, droplet radius bins. All profiles are averaged over the last 3 hours. Panels a/e droplet spectrum, panels b/f - aerosol spectrum, panels c/g cloud water mixing ration profile, panels d/h - cloud droplet number profiles.